Advanced single-slice rebinning for tilted spiral cone-beam CT

Marc Kachelrieß[a] and Theo Fuchs
Institute of Medical Physics, University of Erlangen—Nürnberg, Germany

Stefan Schaller
Siemens AG, Medical Engineering Group, Forchheim, Germany

Willi A. Kalender
Institute of Medical Physics, University of Erlangen—Nürnberg, Germany

(Received 20 November 2000; accepted for publication 18 March 2001)

Future medical CT scanners and today's micro CT scanners demand cone-beam reconstruction algorithms that are capable of reconstructing data acquired from a tilted spiral trajectory where the vector of rotation is not necessarily parallel to the vector of table increment. For the medical CT scanner this case of nonparallel object motion is met for nonzero gantry tilt: the table moves into a direction that is not perpendicular to the plane of rotation. Since this is not a special application of medical CT but rather a daily routine in head exams, there is a strong need for corresponding reconstruction algorithms. In contrast to medical CT, where the special case of nonperpendicular motion is used on purpose, micro CT scanners cannot avoid aberrations of the rotational axis and the table increment vector due to alignment problems. Especially for those micro CT scanners that have the lifting stage mounted on the rotation table (in contrast to setups where the lifting stage holds the rotation table), this kind of misalignment is equivalent to a gantry tilt. We therefore generalize the advanced single-slice rebinning algorithm (ASSR), which is considered a very promising approach for medical cone-beam reconstruction due to its high image quality and its high reconstruction speed [Med. Phys. **27**, 754–772 (2000)], to the case of tilted gantries. We evaluate this extended ASSR approach (which we will denote as ASSR$^+$, for convenience) in comparison to the original ASSR algorithm using simulated phantom data for reconstruction. For the case of nonparallel object motion ASSR$^+$ shows significant improvements over ASSR, however, its computational complexity is slightly increased due to the broken symmetry of the spiral trajectory. [DOI: 10.1118/1.1373675]

Key words: multislice spiral CT (MSCT), micro CT, cone-beam CT, area detector systems, 3-D reconstruction, gantry tilt

I. INTRODUCTION

CT scans with tilted gantries are performed daily in a clinical routine. In contrast to sequence scans and single-slice spiral scans the use of modern multislice spiral scanners requires new reconstruction concepts to compensate for the fact that the rotational axis of the gantry deviates from the axis of table increment by the gantry tilt angle τ. Although special z-interpolation algorithms that account for the gantry tilt problem in an approximate way have recently been developed for four-slice CT scanners[1] there are no specific algorithms yet to be used at higher cone angles and none that incorporate the gantry tilt without applying approximations.

We therefore generalize the approximate cone-beam reconstruction algorithm ASSR (Advanced single-slice rebinning[2]), a very promising candidate for medical CT,[3–5] to the case of tilted gantries. For convenience, we will denote this new extension as ASSR$^+$ (ASSR plus gantry tilt). Although the necessary changes require a complete reformulation of the reconstruction problem, the basic idea remains the same: the spiral trajectory is approximated by a set of overlapping and optimally tilted reconstruction planes along which data of a virtual parallel scanner are synthesized from the measured cone-beam data via rebinning and reconstructed with a standard two-dimensional (2-D) reconstruction technique (e.g., filtered backprojection, Fourier reconstruction, or iterative methods).[2,6] The stack of resulting tilted images is interpolated along the table increment direction $\mathbf{d}$ (d interpolation) to yield the volume on the desired x-y-d-grid.[7] As usual, the z axis is defined to be perpendicular to the x-y plane (scan plane) and coincides with the rotational axis of the scanner.

All advantages of the original ASSR algorithm remain for ASSR$^+$: The images are of high quality, 2-D reconstruction software or hardware can be used for ASSR$^+$ and the formulation as a rebinning approach allows us to incorporate scanner misalignments directly into the reconstruction without the need for an intermediate resampling of the data.[7] These misalignmens may include tilted or skewed detectors and even distorted detectors, as it is the case with image intensifiers. Above all, the gantry tilt is equivalent to a misaligned table increment axis and, consequently, corresponding cases are explicitly covered with ASSR$^+$. In the case of $\tau=0$, ASSR$^+$ is equivalent to ASSR; the d interpolation reduces to a z interpolation.

In this paper we will present the theoretical derivations necessary to adopt ASSR to the case of nonperpendicular

table motion. Since all manipulations, including those that differ between ASSR and ASSR$^+$, are numerically performed with high precision without additional resampling, it turns out that all image quality parameters and figures of merit (e.g., slice sensitivity profiles, image noise, resolution, etc.) remain the same as for the original ASSR. Thus, we will not present corresponding results. The reader is rather referred to Ref. 2.

II. MATERIALS AND METHODS

The notation used here conforms with Ref. 2 as far as possible. The projection angle is called α and will be used to parametrize the complete spiral trajectory, and thus we have $\alpha \in \mathbb{R}$. The angle within the fan is given by β; the detector's z coordinate is denoted as b. For the flat panel detector used for our derivations we have the corresponding coordinates u and v. The ray geometry in 2-D parallel geometry is parametrized by ξ for the ray's distance to the origin and ϑ for its angle. Figure 1 shows the in-plane geometry of the cylindrical detector scanner.

Each planar dataset to be rebinned will be centered about a certain angular position α_R that we call the reconstruction position. Notations and definitions used throughout this paper are given below. Most of them depend on the current reconstruction position α_R. For convenience, this dependency is not explicitly stated. The reader should be aware of the implicit dependence on α_R.

The coordinate system used is matched to the scanner's gantry: the z axis coincides with the rotational axis, and x and y are perpendicular to z to give an orthonormal coordinate base. The table increment is given in this base as a vector **d**. Its length d is the value that is called the table increment per rotation in medical CT. In general, this choice of coordinates is optimal for the development of reconstruction algorithms, although in common CT terminology the vector **d** is referred to as the ''z axis.''

a	the R plane's distance to the origin;
α	projection angle, $\alpha \in \mathbb{R}$;
α_R	projection angle about which the reconstruction is centered;
β, b	detector coordinates for the cylindrical detector;
$\cos \epsilon$	length correction factor to account for the angle ϵ between the measured ray and the virtual ray used for reconstruction; see Eq. (12);
d, τ, κ	the table increment vector per 360° rotation and angles to parametrize **d**; see Eq. (3);
Φ	fan angle, $\Phi = 2 \sin^{-1}(R_M/R_F)$;
l'/l	the length correction factor to allow the virtual scanner to be defined in the horizontal x-y plane instead of the R plane; see Eq. (9);
m	the normal vector of the plane containing both the measured ray and the corresponding approximated ray in the R plane; see Eq. (10);
n, γ, φ	the normal vector of the current R plane and angles to parametrize **n**; see Eq. (5);
o	the origin of the current R plane; see Eq. (6);

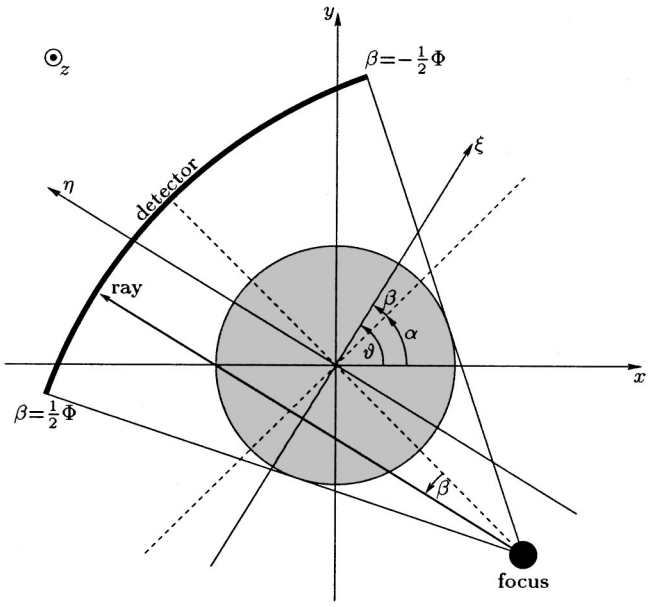

FIG. 1. Coordinate system of a cylindrical detector scanner projected into the x-y plane. The rays are described by the angle β within the fan and the rotation angle α of the gantry in fan geometry. The corresponding parameters in parallel (i.e., rebinned) geometry and ξ and ϑ.

$p(\alpha,u,v)$	the measured projection data at (α,u,v);
$p(\vartheta,\xi)$	rebinned projection data;
r	coordinate vector, $\mathbf{r} = \begin{pmatrix} x \\ y \\ z \end{pmatrix}$;
$\mathbf{r}(u,v)$	coordinates of detector (u,v); see Eq. (2);
$\mathbf{r}(\alpha,u,v)$	beam vector defined as $\mathbf{r}(\alpha,u,v) = \mathbf{r}(u,v) - \mathbf{s}(\alpha)$;
R	the reconstruction plane, defined as $R: \mathbf{n}\cdot\mathbf{r} - a = 0$;
R_D	the distance from detector to center of rotation (z axis), in our case 435 mm;
R_F	the distance from the focus to the center of rotation (z axis), in our case 570 mm;
R_M	the radius of the field of measurement (FOM), in our case 250 mm;
R_{FD}	distance from focus to detector, $R_{FD} = R_F + R_D$;
S	slice thickness;
$\mathbf{s}(\alpha)$	the spiral focus trajectory; see Eq. (1);
ϑ, ξ	beam parameters in parallel geometry. They describe a parallel beam through $\mathbf{o} + \xi\boldsymbol{\xi}(\vartheta)$ with direction $\boldsymbol{\eta}(\vartheta)$;
u, v	detector coordinates for the flat detector;
$\boldsymbol{\xi}$, $\boldsymbol{\eta}$	unit vector pointing from **o** toward the parallel beam (ϑ, ξ) and vector pointing along the beam direction. See Eq. (8);
$\boldsymbol{\xi}'$	normal vector of the plane containing the horizontal virtual ray (ϑ, ξ) and its projection along **d** onto the reconstruction plane, $\boldsymbol{\xi}' = \boldsymbol{\eta} \times \mathbf{d}$;
Δ_{mean}	average deviation of the focus from the reconstruction plane;

(C/W) window setting of the reconstructed images in HU. C is the window center, W the window width.

Spiral cone-beam data were simulated using a dedicated x-ray simulation tool (ImpactSim, VAMP GmbH, Möhrendorf, Germany) and the same scanner geometry (corresponding to the Siemens SOMATOM Volume Zoom) as in Ref. 2. Phantom definitions were taken from the world-wide phantom data base at http://www.imp.uni-erlangen.de/forbild. All reconstruction algorithms were implemented on a standard PC with dedicated image reconstruction and evaluation software (ImpactIR, VAMP GmbH, Möhrendorf, Germany); reconstruction time is below 5 s per image on a 450 MHz Pentium CPU with 256 MB of memory.

III. ADJUSTING THE RECONSTRUCTION PLANE

Our derivations will be based on a flat detector geometry that can be easily transformed to cylindrical detector coordinates necessary to describe the medical CT scanner used for the simulations.[2] The spiral focus trajectory $\mathbf{s}(\alpha)$ and the detector position $\mathbf{r}(u,v)$ are given as

$$\mathbf{s}(\alpha)=R_F\begin{pmatrix}\sin\alpha\\-\cos\alpha\\0\end{pmatrix}+\mathbf{d}\frac{\alpha}{2\pi}, \tag{1}$$

$$\mathbf{r}(u,v)=R_D\begin{pmatrix}-\sin\alpha\\\cos\alpha\\0\end{pmatrix}+u\begin{pmatrix}\cos\alpha\\\sin\alpha\\0\end{pmatrix}+v\begin{pmatrix}0\\0\\1\end{pmatrix}+\mathbf{d}\frac{\alpha}{2\pi}. \tag{2}$$

A plot illustrating the geometry is given in Fig. 2 for the case $\mathbf{d}\|\mathbf{z}$.

Below we will use the following representations of the table increment vector:

$$\mathbf{d}=\begin{pmatrix}d_1\\d_2\\d_3\end{pmatrix}=d\begin{pmatrix}\sin\tau\cos\kappa\\\sin\tau\sin\kappa\\\cos\tau\end{pmatrix}. \tag{3}$$

In medical CT the angle τ is the gantry tilt angle and the value of κ is 90° corresponding to tilting the gantry about the x axis of the scanner.

We now want to find a reconstruction plane R, defined as $R:\mathbf{n}\cdot\mathbf{r}-a=0$, with $\mathbf{n}^2=1$ that optimally fits to a given 180° segment centered about the reconstruction position α_R of the spiral trajectory. Therefore, we simply minimize the mean square distance to the spiral source trajectory, i.e., we minimize

$$\Delta^2_{\text{mean}}=\frac{1}{\pi}\int_{\alpha_R-\pi/2}^{\alpha_R+\pi/2}d\alpha[\mathbf{n}\cdot\mathbf{s}(\alpha)-a]^2.$$

This can be achieved by regarding the derivative with respect to a:

$$\int_{\alpha_R-\pi/2}^{\alpha_R+\pi/2}d\alpha[\mathbf{n}\cdot\mathbf{s}(\alpha)-a]=0.$$

From there follows a as

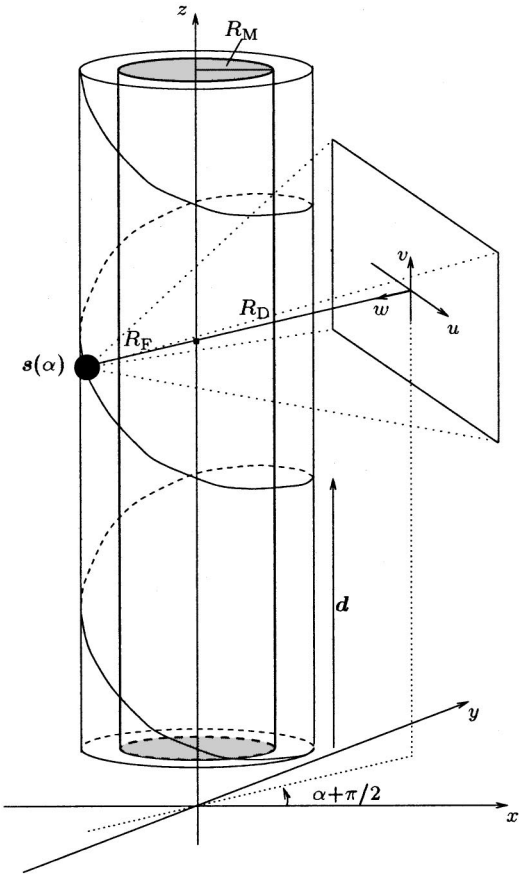

FIG. 2. Cone-beam coordinate system. The vector **d** is the table increment vector, α is the rotation angle, and R_F, R_D, R_M are the distances of the focal spot, of the detector, and of the edge of the FOM, respectively, to the center of rotation.

$$a=\mathbf{n}\cdot\left(\frac{2}{\pi}R_F\begin{pmatrix}\sin\alpha_R\\-\cos\alpha_R\\0\end{pmatrix}+\mathbf{d}\frac{\alpha_R}{2\pi}\right).$$

Inserting this result into the minimization integral gives

$$\Delta^2_{\text{mean}}=\frac{1}{\pi}\int_{\alpha_R-\pi/2}^{\alpha_R+\pi/2}d\alpha[\mathbf{n}\cdot\Delta\mathbf{s}(\alpha)]^2,$$

with

$$\Delta\mathbf{s}(\alpha)=\mathbf{s}(\alpha)-\frac{2}{\pi}R_F\begin{pmatrix}\sin\alpha_R\\-\cos\alpha_R\\0\end{pmatrix}-\mathbf{d}\frac{\alpha_R}{2\pi}.$$

To determine the normal vector $\mathbf{n}$ we need to integrate the mixed components of $\Delta\mathbf{s}$. Thus we define the symmetric 3×3 matrix $\mathbf{S}$ as

$$S_{ij}=\frac{1}{\pi}\int_{\alpha_R-\pi/2}^{\alpha_R+\pi/2}d\alpha[\Delta\mathbf{s}(\alpha)]_i[\Delta\mathbf{s}(\alpha)]_j,$$

such that $\Delta^2_{\text{mean}}=\mathbf{n}^T\cdot\mathbf{S}\cdot\mathbf{n}$. The explicit expressions are

$$48\pi^2S_{11}=\pi^2d_1d_1+24R_F^2(\pi^2-4)+96R_Fd_1\cos\alpha_R+96R_F^2\cos2\alpha_R,$$

$$48\pi^2 S_{12} = \pi^2 d_1 d_2 + 48 R_F (d_1 \sin\alpha_R + d_2 \cos\alpha_R) + 96 R_F^2 \sin 2\alpha_R,$$

$$48\pi^2 S_{13} = \pi^2 d_1 d_3 + 48 R_F d_3 \cos\alpha_R,$$

$$48\pi^2 S_{22} = \pi^2 d_2 d_2 + 24 R_F^2 (\pi^2 - 4) + 96 R_F d_2 \sin\alpha_R - 96 R_F^2 \cos 2\alpha_R,$$

$$48\pi^2 S_{23} = \pi^2 d_2 d_3 + 48 R_F d_3 \sin\alpha_R,$$

$$48\pi^2 S_{33} = \pi^2 d_3 d_3.$$

The constraint $\mathbf{n}^2 = 1$ can be incorporated into the minimization equation using the Langrange method, i.e., by adding $\lambda(\mathbf{n}^2 - 1)$ to the integral. The solution then yields the eigenvalue problem

$$\mathbf{S}\cdot\mathbf{n} = \lambda\mathbf{n}. \tag{4}$$

Multiplying $\mathbf{n}^T$ to the left shows that $\Delta^2_{\text{mean}} = \lambda$ and, consequently, $\mathbf{n}$ must be the eigenvector to the smallest of the three eigenvalues. Equation (4) cannot be reasonably solved analytically. The solution will be performed numerically by evaluating the characteristic polynomial of $\mathbf{S}$ and solving for the eigenvector corresponding to the smallest zero of this characteristic polynomial.

In the tilted spiral Δ_{mean} and the relative orientation of the R planes (relative with respect to the reconstruction position α_R) will vary slightly as a function of α_R. These variations increase with increasing gantry tilt, but even for gantry tilt angles of up to 30° the relative deviation from the mean value turns out to be in the order of 10^{-3}. Although we did not do so one can, in principle, neglect the impact of the gantry tilt on the calculation of the R plane.

Since the reconstruction plane is now determined for a given reconstruction position α_R, we can start with the rebinning procedure where we assume the R plane's normal vector to be represented as

$$\mathbf{n} = \begin{pmatrix} \sin\gamma\cos\varphi \\ \sin\gamma\sin\varphi \\ \cos\gamma \end{pmatrix}. \tag{5}$$

IV. RECONSTRUCTION

Our aim is to synthesize data corresponding to the rays (ϑ,ξ) of a parallel scanner that rotates in the x-y plane. The projection of the virtual scanner's rays along the table increment vector $\mathbf{d}$ corresponds to a parallel scanner with a nonequidistant sampling rotating in R; its line integrals can be taken from the measured cone-beam data by appling only tiny approximations. The advantage of having a virtual scanner rotating in the x-y plane is that reconstructions of data thereof yield the images on the correct x-y grid and interpolations in these two dimensions can be avoided when computing the final volume in Cartesian coordinates. (In contrast to Ref. 2, we avoid having two different rotating coordinate systems, for convenience.)

Our virtual parallel scanner shall be centered about the intersection of the table increment line $\mathbf{d}\mathbb{R}$ and the reconstruction plane, i.e., about the origin,

$$\mathbf{o} = \mathbf{d}\frac{a}{\mathbf{n}\cdot\mathbf{d}}. \tag{6}$$

Moreover, this virtual parallel scanner must allow us to reconstruct the images in world coordinates, i.e., corresponding to a rectangular grid parallel to the x-y plane, centered about $\mathbf{o}$. The problem is to optimally synthesize a ray (ϑ, ξ) of angle ϑ and distance ξ (from $\mathbf{o}$) in the x-y plane using the available cone-beam data. The images resulting from a 2-D reconstruction of these parallel data represent the attenuation values along the reconstruction plane but shall already have the correct x and y coordinates such that image domain interpolations to gain images parallel to x and y remain to be done in the d direction only (note that images shall be centered about the d and not the z axis). A graphical version of the requirements is depicted in Fig. 3(a) showing the horizontal plane of the virtual parallel scanner, some discrete samples thereon, and the tilted R planes with the corresponding samples.

To solve the task we start from the ray (ϑ,ξ) in the x-y plane and calculate its projection along the table increment vector $\mathbf{d}$ onto the reconstruction plane [see Figs. 3(a) and 3(b)]. This can be formulated as the intersection of the R plane $\mathbf{n}\cdot\mathbf{r} - a = 0$ with the plane

$$(\boldsymbol{\eta}\times\mathbf{d})\cdot(\mathbf{r} - \xi\boldsymbol{\xi} - \mathbf{o}) = 0, \tag{7}$$

which is spanned by the virtual parallel ray (i) and the table increment vector. Thereby, we have introduced the unit vector $\boldsymbol{\xi}$ pointing from $\mathbf{o}$ to the ray (ϑ,ξ) and the ray's direction vector $\boldsymbol{\eta}$:

$$\boldsymbol{\xi} = \boldsymbol{\xi}(\vartheta) = \begin{pmatrix} \cos\vartheta \\ \sin\vartheta \\ 0 \end{pmatrix},$$
$$\boldsymbol{\eta} = \boldsymbol{\eta}(\vartheta) = \begin{pmatrix} -\sin\vartheta \\ \cos\vartheta \\ 0 \end{pmatrix}, \quad \text{with} \quad \boldsymbol{\xi}\times\boldsymbol{\eta} = \mathbf{z}. \tag{8}$$

The situation is illustrated in Fig. 3(b), where the lines (i), (ii), and (iii) correspond to the parallel rays in the x-y plane, to their projection onto the reconstruction plane, and to the measured ray, respectively.

For convenience, we will further use the abbreviation

$$\boldsymbol{\xi}' := \boldsymbol{\eta}\times\mathbf{d},$$

which can be precomputed and stored for all ϑ's of interest. Using $\boldsymbol{\xi}'\cdot\boldsymbol{\xi} = d_3$ and $\boldsymbol{\xi}'\cdot\mathbf{o} = 0$ allows us to reformulate the plane (7) as

$$\boldsymbol{\xi}'\cdot\mathbf{r} = \xi d_3.$$

The line of intersection (ii) of both planes is perpendicular to their normal vectors $\mathbf{n}$ and $\boldsymbol{\xi}'$ and thus has the direction $\mathbf{n}\times\boldsymbol{\xi}'$. Since the transformation from parallel raw data in the R plane to the data finally used for reconstruction in the horizontal plane must be exact, we have to apply a length

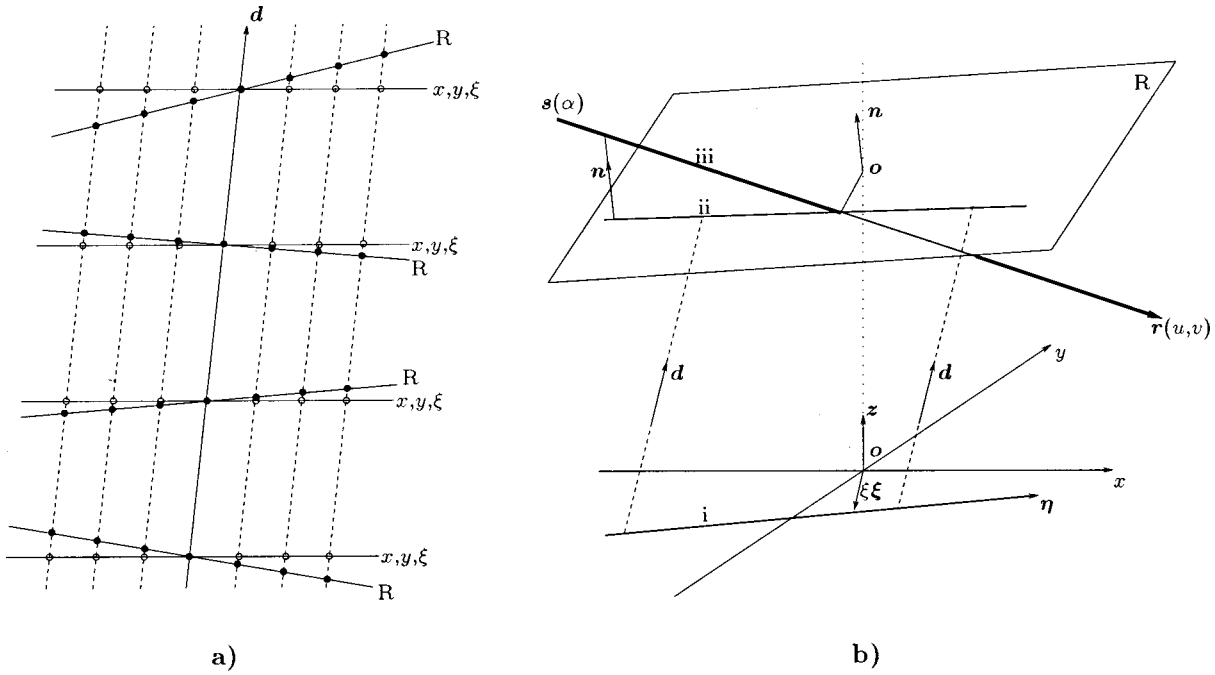

FIG. 3. (a) The 2D plot illustrating the interpolations along **d** for four arbitrarily selected *R* planes. The points to be reconstructed and the parallel rays to be synthesized correspond to the solid circles. The hollow circles depict the geometry of the virtual parallel scanner that is living in the *x-y* plane to remain constant from *R* plane to *R* plane. (b) A given ray in parallel coordinates (i) is projected along **d** onto the *R* plane, resulting in the virtual ray (ii) assumed to be available for reconstruction. The corresponding measured ray (iii) will be found by intersecting the source trajectory with a plane containing (ii) and the normal vector **n** of the reconstruction plane *R*. The detector coordinates of (iii) are given by minimizing the mean distance of the ray from the *R* plane. Although the origin of the *x-y* plane coincides with the origin of the *R* plane we have moved them apart for illustration purposes and, consequently, **o** appears twice.

correction to the transformed values. At first go, one would assume the cosine of the angle between the vector $\mathbf{n}\times\boldsymbol{\xi}'$ and the vector $\boldsymbol{\eta}$ to be the correct factor. However, this would be true only if the tilted ray was projected orthogonally into the horizontal plane. Here, we rather deal with a projection along **d**. This requires a more complicated length correction that is illustrated in Fig. 4.

From there it becomes clear that the length correction ratio l'/l can be calculated by regarding the vector sum

$$l'\,\boldsymbol{\eta}+\mathbf{d}=l\,\frac{\mathbf{n}\times\boldsymbol{\xi}'}{|\mathbf{n}\times\boldsymbol{\xi}'|}.$$

Multiplying by $\boldsymbol{\xi}'\times\mathbf{d}$ yields

$$\frac{l'}{l}=\frac{(\mathbf{n}\times\boldsymbol{\xi}')\cdot(\boldsymbol{\xi}'\times\mathbf{d})}{|\mathbf{n}\times\boldsymbol{\xi}'|\,\boldsymbol{\eta}\cdot(\boldsymbol{\xi}'\times\mathbf{d})}$$

$$=\frac{\mathbf{n}\cdot\mathbf{d}}{|\mathbf{n}\times\boldsymbol{\xi}'|}=\frac{d(\cos\gamma\cos\tau+\cos(\kappa-\varphi)\sin\gamma\sin\tau)}{|\mathbf{n}\times\boldsymbol{\xi}'|}. \quad (9)$$

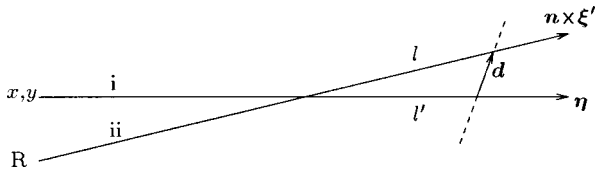

FIG. 4. The length correction l'/l from tilted geometry to horizontal geometry must take the direction **d** into account.

This value must be multiplied to the rebinned parallel data prior to 2-D reconstruction.

A. Focus position

The measured ray to be used, i.e., line (iii) of Fig. 3(b), must lie on a plane through $\mathbf{s}(\alpha)$, which is parallel to **n** and intersects *R* in the virtual ray (ii). This plane is given as $\mathbf{n}\times(\boldsymbol{\xi}'\times\mathbf{n})\cdot[\mathbf{r}-\mathbf{s}(\alpha)]=0$, to which we will further refer as

$$\mathbf{m}\cdot[\mathbf{r}-\mathbf{s}(\alpha)]=0 \quad \text{with} \quad \mathbf{m}=\mathbf{n}\times(\boldsymbol{\xi}'\times\mathbf{n})=\boldsymbol{\xi}'-(\mathbf{n}\cdot\boldsymbol{\xi}')\mathbf{n}. \quad (10)$$

Thus, we seek for the angle α that solves the linear system,

$$\boldsymbol{\xi}'\cdot\mathbf{r}=\xi d\cos\tau,$$

$$\mathbf{n}\cdot\mathbf{r}=a,$$

$$\mathbf{m}\cdot\mathbf{r}=\mathbf{m}\cdot\mathbf{s}(\alpha).$$

As one can easily see from the definition of **m**, the determinant of the system is 0. Subtracting the first equation from the last and adding $\mathbf{n}\cdot\boldsymbol{\xi}'$ times the second equation to the last equation zeros the latter, leaving the transcendental equation,

$$\mathbf{m}\cdot\mathbf{s}(\alpha)-\xi d\cos\tau+(\mathbf{n}\cdot\boldsymbol{\xi}')a=0,$$

which determines the focus position α. To solve it we must bring it into the more practical form

$$dR_F[\sin(\alpha-\vartheta)\cos^2\gamma\cos\tau+A(\alpha)]+\mathbf{m}\cdot\mathbf{d}\frac{\alpha}{2\pi}$$
$$=\xi d\cos\tau-(\mathbf{n}\cdot\boldsymbol{\xi}')a,$$

with

$$A(\alpha)=\sin(\alpha-\varphi)\cos(\kappa-\vartheta)\sin\gamma\cos\gamma\sin\tau$$
$$-\cos(\alpha-\varphi)\sin(\vartheta-\varphi)\sin^2\gamma\cos\tau.$$

This can be solved using Banach's theorem when being rewritten, using $\beta=\vartheta-\alpha$, as

$$\beta=\sin^{-1}\frac{dR_FA(\vartheta-\beta)+\mathbf{m}\cdot\mathbf{d}\frac{\vartheta-\beta}{2\pi}-\xi d\cos\tau+(\mathbf{n}\cdot\boldsymbol{\xi}')a}{dR_F\cos^2\gamma\cos\tau},$$

using two to three fixed point iterations in β only. From $\alpha=\vartheta-\beta$ the focus position α is determined.

This step is the decisive step in tilted spiral reconstruction. If the focus position was derived by neglecting the gantry tilt, severe artifacts would occur.

B. Detector coordinates

The remaining task to solve is to compute the optimal detector coordinates (u,v) for a given source position $\mathbf{s}(\alpha)$ and a given reconstruction plane $R:\mathbf{n}\cdot\mathbf{r}-a=0$. This will be achieved if the mean distance of the respective ray [emerging from $\mathbf{s}(\alpha)$ and ending at the detector at $\mathbf{r}(u,v)$] from the reconstruction plane is zero. However, we must correct for the fact that the detector's distance R_D to the center of rotation generally differs from the focus distance R_F. Thus we simply regard $\mathbf{s}(\alpha)+(2R_F/R_{FD})\mathbf{r}(\alpha,u,v)$ as the ending point of the ray and demand for the distances of the starting and scaled ending point to have opposite sign:

$$[\mathbf{n}\cdot\mathbf{s}(\alpha)-a]+\left[\mathbf{n}\cdot\left(\mathbf{s}(\alpha)+\frac{2R_F}{R_{FD}}\mathbf{r}(\alpha,u,v)\right)-a\right]=0,$$

or, equivalently,

$$\mathbf{n}\cdot\mathbf{r}(\alpha,u,v)=\frac{R_{FD}}{R_F}[a-\mathbf{n}\cdot\mathbf{s}(\alpha)]. \tag{11a}$$

Since the ending point $\mathbf{r}(u,v)$ of the ray must lie on the plane $\mathbf{m}\cdot[\mathbf{r}-\mathbf{s}(\alpha)]=0$ [see Eq. (10)], we further obtain

$$\mathbf{m}\cdot\mathbf{r}(\alpha,u,v)=0. \tag{11b}$$

Due to $\mathbf{m}=\boldsymbol{\xi}'-(\mathbf{n}\cdot\boldsymbol{\xi}')\mathbf{n}$, adding $\mathbf{n}\cdot\boldsymbol{\xi}'$ times Eq. (11a) to Eq. (11b) gives

$$\boldsymbol{\xi}'\cdot\mathbf{r}(\alpha,u,v)=\frac{R_{FD}}{R_F}[a-\mathbf{n}\cdot\mathbf{s}(\alpha)](\mathbf{n}\cdot\boldsymbol{\xi}'). \tag{11c}$$

Taking (11a) and (11c) and simplifying yields

$$u\cos(\alpha-\varphi)\sin\gamma+v\cos\gamma$$
$$=\frac{R_{FD}}{R_F}[c-\mathbf{n}\cdot\mathbf{s}(\alpha)]+R_{FD}\sin(\alpha-\varphi)\sin\gamma,$$

$$u\cos(\alpha-\vartheta)\cos\tau-v\cos(\kappa-\vartheta)\sin\tau$$
$$=\frac{R_{FD}}{R_F}[a-\mathbf{n}\cdot\mathbf{s}(\alpha)](\mathbf{n}\cdot\boldsymbol{\xi}')d^{-1}+R_{FD}\sin(\alpha-\vartheta)\cos\tau.$$

These equations are linear in u and v and can be solved by straightforward inversion.

C. Length correction

Since the virtual rays that are going to be used for reconstruction and their corresponding measured rays differ by a small angle ϵ, we must apply a length correction to yield the correct virtual projection values from the measured attenuation. Fortunately, we already know the sine of the angle of the ray $\mathbf{r}(\alpha,u,v)$ used for reconstruction and the virtual ray assumed to be available for reconstruction: it is given by Eq. (11a). Thus, the correction factor to be applied simply is

$$\cos\epsilon=\sqrt{1-\left(\frac{\mathbf{n}\cdot\mathbf{r}(\alpha,u,v)}{\sqrt{R_{FD}^2+u^2+v^2}}\right)^2}$$
$$=\sqrt{1-\frac{R_{FD}^2[a-\mathbf{n}\cdot\mathbf{s}(\alpha)]^2}{R_F^2(R_{FD}^2+u^2+v^2)}}. \tag{12}$$

D. Reconstruction position and *d* interpolation in the image domain

Since the principles of selecting the reconstruction positions α_R and the principles of the image domain interpolation remain the same as in the case for nontilted gantries the reader is referred to Ref. 2 for details. Since the relative location of the R planes only changes slightly for each α_R there is no reason to analyze a more complicated selection of the reconstruction increment or to develop other interpolation methods. A qualitative description of the procedure is given in the following.

The reconstruction positions α_R are selected equidistantally spaced with a spacing of $\Delta\alpha_R$. The value of $\Delta\alpha_R$ is chosen small enough to ensure that the maximum distance of two adjacent R planes within the FOM plus the mean deviation $(R_M/R_F)\Delta_{\text{mean}}$ of the focal trajectory and the R plane (projected onto the edge of the FOM is smaller than the collimated slice thickness S. This assures S to be the lower limit of achievable z resolution.[2]

The d interpolation is done with a filter approach, for example, using a triangular filter in the d direction. The width of the filter can be chosen to meet certain requirements on the resolution; here, however, we use S as the filter's width only. Since the synthesized data and the reconstructed images have already the correct in-plane coordinates for d filtering, only pixels of the same index of adjacent R planes are addressed for d interpolation. The number of interpolations is thus reduced to a minimum.

V. SUMMARY OF THE RECONSTRUCTION PROCEDURE

To reconstruct a complete volume, we must perform the following steps for each reconstruction position α_R.

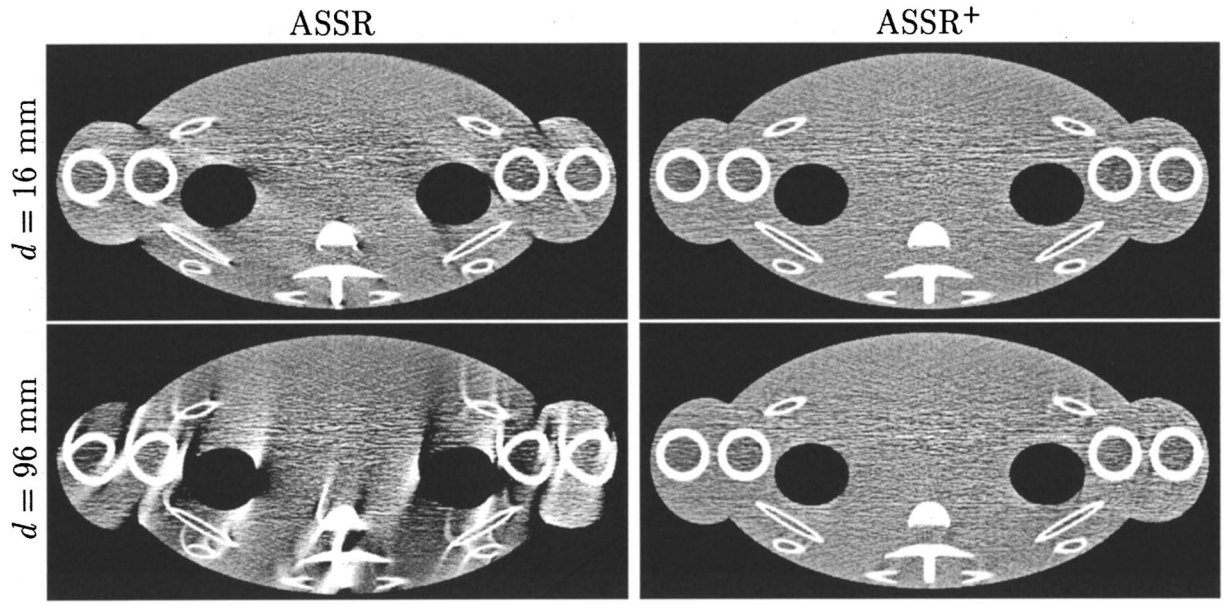

FIG. 5. A comparison of ASSR and ASSR$^+$ at a gantry tilt angle of 30°. Here, it becomes obvious that neglecting the gantry tilt yields unacceptable images. (0/200).

(i) Calculate the optimal R plane.
(ii) For each $\vartheta \in \alpha_R + [-\pi, \pi)$ and each $\xi \in [-\frac{1}{2}R_M, \frac{1}{2}R_M]$ rebin as follows:

- Calculate the length correction l'/l between rays in R and those in the x-y plane.
- Compute the focus position α as a function of ϑ and ξ.
- Compute the detector coordinates (u,v) as a function of ϑ, ξ and α.
- From α, u, and v calculate the length correction $\cos\epsilon$ to account for the angle between the physical ray and its correspondent ray in the reconstruction plane.
- If other misalignments than the gantry tilt, e.g., a perspective transformation, must be corrected for, compute the corresponding new coordinates u' and v', otherwise use $u'=u$ and $v'=v$. This may also include the transformation to cylindrical detector coordinates.
- Assign $p(\vartheta,\xi)=(l'/l)\cos\epsilon\, p(\alpha,u',v')$ to build up the parallel sinogram. Since the measured data are discrete, this requires an interpolation in the coordinates α, u, and v. Although more sophisticated methods may be adequate, we use a simple trilinear interpolation.

(iii) Reconstruct the 2-D data $p(\vartheta,\xi)$ to yield the object cross section along the current R plane.

The remaining step is to do the d interpolation of a stack of reconstructed, tilted images. Since we have taken care that the parallel geometry remains constant in the x-y plane for all α_R by consequently using geometric projections along **d** only, this procedure will not require us to interpolate between neighboring pixels of one image. The d interpolation rather takes place between adjacent tilted images and only accesses pixels of the same index.

VI. RESULTS

Although evident, we first want to explicitly emphasize the necessity of the generalization ASSR$^+$ in comparison to ASSR when using data obtained with a tilted gantry. Therefore, Fig. 5 shows reconstructions of the thorax phantom with $\tau=30°$ performed (a) with ASSR disregarding the fact that the gantry was tilted and (b) with ASSR$^+$, which properly takes τ into account. Clearly, only ASSR$^+$ achieves optimal image quality for all situations and, clearly, the reconstructions neglecting the gantry tilt are not of diagnostic value.

The performance of the generalized version ASSR$^+$ is slightly reduced as compared to the former ASSR algorithm. The reason is that the weights needed for rebinning cannot be stored into lookup tables that typically rely on the spiral rotational/translational symmetry. This symmetry allows us to compute tables for one α_R only and use the tables for other reconstruction positions since any angular increment is equivalent to a translation in z. If $\tau\neq 0$ this equivalence does not hold anymore, the symmetry of the spiral is broken and the table generation would have to be performed for each α_R (modulo 360°), which would require too much memory. However, we only observed a decrease of 10% in reconstruction speed, which we regard as acceptable.

To evaluate the ASSR$^+$ performance we have performed the same experiments as for ASSR.[2] As expected, the results achieved with the new algorithm do not differ from the standard ASSR approach. The image noise values, the MTF (modulation transfer function) and the SSPs (slice sensitivity profiles) remain the same, even when tilting the gantry as

TABLE I. The number of detector slices M used for reconstruction as a function of the table increment value and the gantry tilt angle. The slice thickness used is $S=1$ mm; the fan angle of 52° covers a 500 mm FOM.

d	$\tau=0°$	$\tau=10°$	$\tau=30°$
16 mm	12	12	10
96 mm	69	68	61

much as $\tau=30°$. This is no surprise, since the number of interpolations has not increased as compared to ASSR. The main difference is that the rays are selected slightly more sophisticated to account for the broken symmetry due to the nonperpendicular table motion.

Of course, care has to be taken about how the table increment values have been defined. A given absolute table increment value d yields a z component of $d\cos\tau$, and thus the degree of overlap varies with the gantry tilt. For example, a scan with $d=96$ mm will result in a z component of $d_3 \approx 83$ mm when scanning with $\tau=30°$. The number of required detector slices will go down with increasing gantry tilt as well. In this example the scanner tilted by 30° utilizes $M=61$ detector slices (assuming $S=1$ mm) whereas the simulated scan with $\tau=0°$ and $d=96$ mm needs $M=69$ slices. The pitch value is $p=d_3/MS\approx 1.4$ for both cases. These correspond to a full body FOM of 500 mm diameter and a fan angle of $\Phi=52°$. The complete values for all simulations performed are given in Table I.

Reconstructed images allow us to compare the images qualitatively and to evaluate the artifact content. We have simulated data corresponding to spiral scans with $d=16$ mm and 96 mm with gantry tilts of $\tau=0°$, 10°, and 30°. The polar angle κ was chosen as 90° to correspond to a tilt about the x axis. The results, however, apply to arbitrary polar angles since κ only introduces a relative angular shift of the scan. Figure 6 shows the qualitative behavior of ASSR and ASSR$^+$. Due to the different orientation of the primary, reconstructed sections, it has become necessary to depict oblique multiplanar reformations (tilted by $-\tau$), which then show the same slice as for the case $\tau=0$. As expected, there are no significant differences between the extended approach and standard ASSR. This indicates that ASSR$^+$ is quantitatively and qualitatively equivalent to ASSR and, in addition, also allows us to reconstruct data for $\tau\neq 0$. The amount of gantry tilt used does not influence the image quality.

A precise inspection of these six images, however, reveals slight differences. Especially the artifact behavior around the four ribs in the $d=96$ mm data seems to vary. And the two ribs—they appear as small triangles at the bottom of the images—emerging directly below the vertebra seem to be depicted inconsistently. The explanation is that those artifacts depend on the absolute tube angle and thus on the gantry angle at scan start (a fact that has already been observed and demonstrated for ASSR[2]). Additionally, the images for $\tau\neq 0$ represent MPRs and not the primary reconstructed slice. Although care has been taken when computing these MPRs, the depicted slices are of slightly different effective thickness and, consequently, objects partially reaching into the slice (such as the two ribs) will be depicted inconsistently. And third, artifacts, such as streaks, tend to stay within the primary reconstructed slice. These slices correspond to the R planes and, consequently, are followed by d interpolation that suppresses the artifacts due to the combination of different primary slices. This combination by d interpolation differs for the axial slices and the MPRs, which explains the slight different artifact behavior of the images. Apart from these well-understood effects there are no differences between ASSR images for $\tau=0$ and $\tau\neq 0$.

VII. DISCUSSION

We have extended the applicability of the advanced single-slice rebinning approach to the case of tilted gantries. The generalized algorithm ASSR$^+$ combines the advantages of the standard ASSR approach with the ability to use data from scans with nonparallel object motion. As an extension of ASSR, ASSR$^+$ is a promising candidate for future medical CT image reconstruction. It achieves high image quality with optimal computational performance. ASSR$^+$ can be used for all spiral trajectories, including gantry tilt.

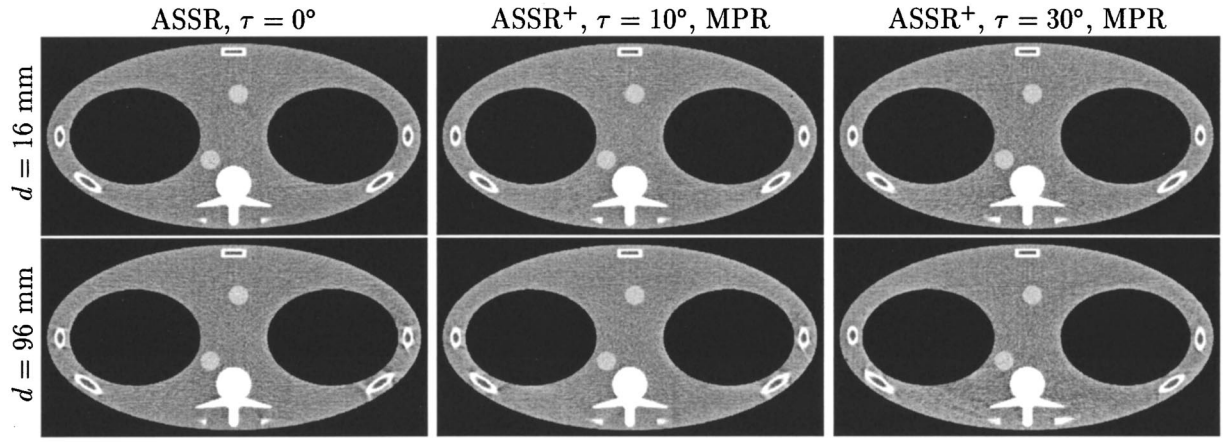

FIG. 6. A comparison of a section of the thorax phantom for various gantry tilts. Due to the different primary sections, the computation of an MPR for the tilted reconstruction is necessary to show the same plane for all cases. Primary sections for the tilted raw data are shown in Fig. 5. (0/200).

As a side effect, ASSR$^+$ seems well suited for micro CT applications as well. Since the algorithm is formulated as a rebinning algorithm, it allows for arbitrary misalignment corrections, such as perspective transformations or simple shifts and rotations of the detector without loss of resolution. The most complicated misalignment to correct for, i.e., the case of a noncoinciding rotational and translational axis, is explicitly taken into account and thus solved by ASSR$^+$ without introducing additional approximations. Thus, all misalignments can be accounted for without additional interpolation and resampling steps.

Because ASSR$^+$ in its present form does not allow for arbitrary pitch values, there have been investigations to generalize the standard ASSR algorithm to this case using spiral interpolation techniques.[5] Alternatively, it may appear more promising to loosen the restriction on the *R* planes and allow greater deviations from the spiral trajectory: accepting less restrictive approximations would additionally allow us to make better use of the available detector area in cases of low pitch. Modifications of ASSR toward the case of arbitrary pitch have been recently published.[8] Extending ASSR$^+$ to the case of arbitrary pitch values is under current investigation and will allow us to cover all spiral scan modes in use today.

In conclusion, ASSR is able to perform high quality reconstructions for today's multislice scanners as well as for future cone-beam scanners. All quantitative measures such as image noise, resolution, etc. remain the same as for the gold standard single-slice spiral CT. We have shown reconstructions using simulated data corresponding to up to 69 simultaneously measured slices without significant artifacts and without a significant increase in reconstruction time. The next generation of medical CT scanners is likely to have up to 16 simultaneous measured slices or more. We assume that the future of medical CT image reconstruction is likely to be of ASSR type.

ACKNOWLEDGMENTS

This work was supported by the ''FORBILD'' Grant No. AZ 286/98 ''Bayerische Forschungsstiftung, München, Germany.''

[a)]Author to whom correspondence should be addressed. Institute of Medical Physics, University of Erlangen—Nürnberg, Krankenhausstraße 12, D-91054 Erlangen, Germany. Telephone: ..49-9131-8522957; fax: ..49-9131-8522824; electronic mail: marc.kachelriess@imp.uni-erlangen.de

[1] J. Hsieh, ''Tomographic reconstruction for tilted helical multislice CT,'' IEEE Trans. Med. Imaging **19**, 864–872 (2000).

[2] M. Kachelrieß, S. Schaller, and W. A. Kalender, ''Advanced single-slice rebinning in cone-beam spiral CT,'' Med. Phys. **27**, 754–772 (2000).

[3] M. Kachelrieß, S. Schaller, and W. A. Kalender, ''Advanced single-slice rebinning in cone-beam spiral CT: Theoretical considerations and medical applications,'' *SPIE Medical Imaging Conference Proceedings*, Vol. 3979, pp. 494–505, 2000.

[4] H. Bruder, M. Kachelrieß, S. Schaller, and T. Mertelmeier, ''Performance of approximate cone-beam reconstruction in multislice computed tomography,'' in Ref. 3, pp. 541–555.

[5] H. Bruder, M. Kachelrieß, S. Schaller, K. Stierstorfer, and T. Flohr, ''Single-slice rebinning reconstruction in spiral cone-beam computed tomography,'' IEEE Trans. Med. Imaging **19**, 873–887 (2000).

[6] G. L. Larson, C. C. Ruth, and C. R. Crawford, ''Nutating slice CT image reconstruction apparatus and method,'' United States Patent 5,802,134, 1998.

[7] M. Kachelrieß and W. A. Kalender, ''Advanced single-slice rebinning (ASSR) and misalignment correction for large cone-beam spiral CT,'' Radiology **217**, 404 (2000).

[8] S. Schaller, K. Stierstorfer, H. Bruder, M. Kachelrieß, and T. Flohr, ''Novel approximate approach for high-quality image reconstruction in helical cone beam CT at arbitrary pitch,'' *SPIE Medical Imaging Conference Proceedings* (in press), 2001.